Angle-resolved X-ray photoelectron spectroscopy intensity modeling of SiNx ultrathin layer grown on Si (100) and Si (111) substrates by N2 plasma treatment

Hiba Beji, Valentin Develay, Guillaume Monier, Luc Bideux, Philip E Hoggan, Angelique Bousquet, Eric Tomasella, Christine Robert-Goumet

Angle-Resolved X-ray Photoelectron Spectroscopy intensity modeling of SiN_x ultrathin layer grown on Si (100) and Si (111) substrates by N_2 plasma treatment

[1,2]Hiba Beji, [1]Valentin Develay, [1] Guillaume Monier, [1]Luc Bideux, [1]Philip E. Hoggan, [2]Angelique Bousquet, [2]Eric Tomasella, [1]Christine Robert-Goumet

[1]Université Clermont Auvergne, Clermont Auvergne INP, CNRS, Institut Pascal, F-63000 Clermont-Ferrand, France

[2]Université Clermont Auvergne, CNRS, Institut de Chimie de Clermont-Ferrand, F-63000 Clermont-Ferrand, France

Corresponding author: Christine.robert-goumet@uca.fr

Keywords:

Ultrathin SiN_x overlayer, Nitridation process, Angle Resolved X-ray Photoelectron Spectroscopy (ARXPS), bi-layer modeling, Diffusion phenomenon, Chemical composition, Thickness measurements.

Abstract:

In this work, we investigate the silicon nitridation process using a N_2 plasma Glow Discharge Source (GDS) in an ultra-high vacuum chamber. In situ Angle Resolved X-ray Photoelectron Spectroscopy (ARXPS) measurements were performed to determine various chemical environments of the surface species. The main goals of this study are determination of the film chemical composition, to estimate its thickness and identify various phenomena taking place during the nitridation process under different experimental conditions. To achieve

these objectives, we developed an ARXPS intensity model for an ultrathin SiN_x overlayer. Based on the ARXPS results, which indicate that the silicon nitride film is not homogenous, we adopted a bi-layer model composed of two $Si_xN_yO_z$ layers with varying thickness and chemical composition. The model is built from analysis of photoelectron intensities, considering a comparison between experimental and theoretical data. This bi-layer model revealed that the silicon nitride layer consists of a surface layer composed of approximately equal amounts of silicon and nitrogen (50% each), and an interfacial layer containing varying amounts of oxygen depending on experimental parameters. The presence of oxygen is due to residual air contamination in the vacuum chamber and/or to Si native oxide. The estimated thickness of silicon nitride film is less than 9 nm, depending on the nitridation time and temperature.

The model developed in this work enabled us to study the effects of initial surface state (as received or chemically cleaned), Si substrate crystallographic orientation (such as (100) and (111)), and the nitridation temperature (room temperature and 500°C). The diffusing species (N^+, N_2^+, O^+), which play a crucial role during nitridation, were found to be influenced by temperature, treatment time, and substrate orientation. The diffusion phenomenon competed with other processes such as NO desorption, leading to a significant impact on formation of the SiN_x film. Furthermore, we compared the thickness obtained from the ARXPS model using cross-sectional High-Resolution Transmission Electron Microscopy (HR-TEM) images. Additional Low-Energy Electron Diffraction (LEED) measurements indicated that the SiN_x film was amorphous.

1. Introduction:

The oldest and most prevalent generation of photovoltaic (PV) technologies relies on silicon semiconductors. Currently, the production of silicon cells dominates the PV cell market and is expected to maintain its dominance due to silicon being an abundant, inexpensive and readily available raw material [1,2]. Enhancements in the efficiency of silicon solar cells are achieved through the application of an anti-reflective coating [3]. However, the growth process of this anti-reflective coating creates different types of defects at the interface such as those caused by ion bombardment during Plasma Enhanced Chemical Vapor Deposition (PECVD) [4–6]. This damage leads to a high density of interface states, ultimately resulting in reduced solar cell efficiency.

One approach to tackle this problem is incorporating a buffer layer to minimize the recombination of photo-generated carriers at the interface. Indeed, Jan Schmidt *et al.* [7] have investigated the growth of a thin thermal SiO_2 layer interposed between Si and the SiN_x film. These authors have shown that the higher thermal budget of SiN_x/SiO_2 stacks, compared to the single-layer SiN_x films, leads to a degradation of the bulk carrier lifetime in silicon. Chunlan Zhou *et al.*[8] have demonstrated that the insertion of a thin SiO_yN_x layer at the interface of SiN_x/Si leads to decrease in the density of interface states. A thin silicon nitride layer has emerged as a strong contender to replace thermal silicon dioxide due to its superior impurity diffusion barrier properties, higher density, and dielectric constant. These ultra-thin silicon nitride buffer layers can be prepared by several methods: Nitrogen ion implantation at high and low energy[9–11], nitridation using N_2 molecules by reaction at high temperature (≥1000°C)[12–14], nitridation using NH_3 gas at relatively low temperatures

(625°C) [15,16], thermal nitridation [900°C – 1200°C] using pure ammonia NH_3 and NH_3-Ar mixtures [17] and by LPCVD (Low Pressure Chemical Vapor Deposition) using silane (SiH_4) and ammonia (NH_3)[18].

However, these techniques of manufacture lead to various problems. For instance, thin film deposition processes using toxic gases like silane (SiH_4) [18] pose health risks and are potentially dangerous for the environment, but are effective for passivating the silicon defects. Other synthetic processes involving high temperatures [12–14], lead to an increase in production costs and to a decline in the performance of semiconductor devices. The plasma nitriding processes using NH_3 can degrade the semiconductor material due to hydrogen inclusion. In addition, processes known as ion implantation, with a high ion energy between 12-20 keV, generate damage to the Si substrate, resulting in the formation of a deformed crystalline structure at the SiN_x/Si interface [19]. To notably mitigate potential hydrogen-induced damage, plasma nitridation using N_2 is an effective means of creating a silicon oxynitride layer with a high nitrogen content. In this work, we propose to modify the Si surface by a low-power plasma N_2 treatment at low temperature (T≤500°C). *In situ* Angle Resolved X-ray Photoelectron Spectroscopy (ARXPS) is used to determine the depth composition and the thickness of silicon nitride films. The goal of this study is to control the growth of SiN_x buffer layer created by soft N_2 plasma nitridation under different experimental conditions. Thus, this study highlights the benefits of *in situ* ARXPS elucidating the phenomenological study of the silicon nitridation process. To validate the accuracy of the thickness estimated by our ARXPS intensity model, additional High-Resolution Transmission Electron Microscopy (HR-TEM) measurements were performed.

2. Experimental part:

The experiments were performed on n-type Si (100) and Si (111) substrates with phosphorus doping for a resistivity of 10 Ω.cm. Two series of samples have been studied: - Si surfaces which did not undergo any preparation, named “as-received,” and - Si surfaces chemically cleaned with 1% hydrofluoric acid solution to remove surface contamination, named “cleaned,” before their loading into the Ultra High Vacuum chamber (10^{-8} Pa).

The two sets of Si samples have been nitrided using a N_2 Glow Discharge Source (GDS) working at low power (5 W), with N_2 gas (purity N6.0) at a pressure of 10^{-3} Pa. The nitrogen molecules N_2 are dissociated by a potential difference of 2.5 kV. The GDS source produces species mostly in the ionic state (N^+, N^{2+}). Current density on the sample is recorded as about 2 $\mu A/cm^2$. Two nitridation temperatures have been used: room temperature (RT) and 500°C.

Before and after the nitridation process, the samples are studied by Angle Resolved X-ray Photoelectron Spectroscopy (ARXPS) using an OMICRON EA125 analyzer and a non-monochromatic Mg Kα (1253.6 eV) source, at a pass energy of 20 eV. For fitting X-ray photoelectron spectra, the Gaussian-Lorentzian function and Shirley background are used [20] [21]. After surface nitridation, as no C1s contamination peak is recorded, the binding energy of the N1s peak (398.1 eV) was used to calibrate the binding energy scale. As discussed below, this was to correct the possible energy shifts due to charge effects. As surface sensitivity is increased by varying the photoelectron emission angle, photoelectron spectra are acquired for selected emission angles: 0°, 20°, 40° and 60° versus surface normal.

To investigate the crystallinity of the SiN_x film, low-energy electron diffraction (LEED) technique was performed. Cross sectional HR-TEM images were carried out using a JEM-

2100 PLUS instrument equipped with a 200 kV operating source, after a Focused Ion Beam (FIB) preparation using Xe ions. To efficiently protect the synthesized nitride films, an interstitial carbon protection layer was used.

3. Methodology and calculation:

3.1 ARXPS spectra decomposition methodology:

Before performing the nitridation process, the initial surfaces were analysed by X-ray Photoelectron Spectroscopy (XPS) (figure 1). The Si2p peak was decomposed using a spin-orbit splitting of 0.6 eV between the $Si2p_{1/2}$ and $Si2p_{3/2}$ contributions [22]. In all this work, the photoelectron doublet of Si2p is decomposed as a single envelope that combines the two peaks $2p_{1/2}$ and $2p_{3/2}$. As shown in figure 1, the as-received samples which do not undergo any preparation revealed surface native oxidation. One peak is ascribed to $Si\text{-}Si_4$ bonds at BE = 99.6 eV [23] corresponding to the signal coming from the Si substrate. And the other peak at BE = 103.6 eV is attributed to $Si–O_4$ bonds [23] corresponding to the signal arising from the surface contamination layer. The SiO_2 thickness has been estimated by XPS intensitiy modeling [24,25] at around 1.1 nm on both Si (100) and Si (111) surfaces. Concerning the chemically cleaned Si surfaces, no Si-O contribution to Si2p has been recorded for either of these crystallographic orientations.

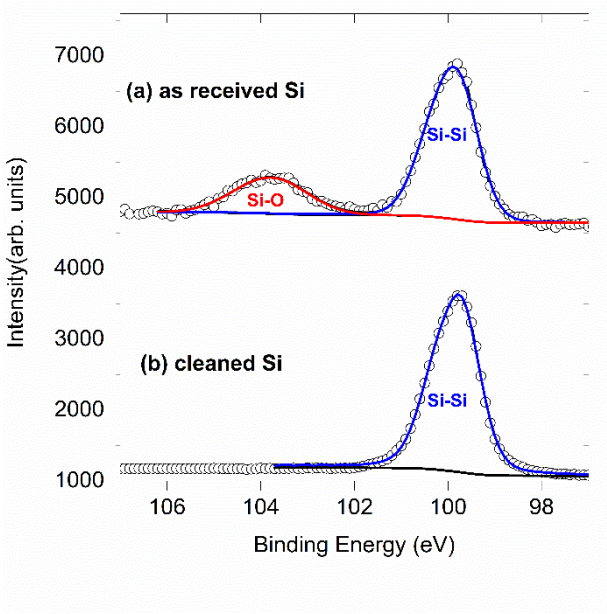

Figure 1: XPS Si2p spectra before nitridation for (a) as received and (b) cleaned silicon (100) substrate.

After nitridation process at RT for 1h on the two sets of Si (100) substrates, decompositions of Si2p, N1s and O1s spectra are shown in figure 2. The nitridation process leads to the broadening of the Si2p peak which is ascribed to the formation of new chemical states and the appareance of a N1s peak. Moreover, the presence of O1s peak at a binding energy (BE) of 532.6 eV reveals a residual oxygen contamination during the nitridation process as observed in previous work [26,27]. As the nitridation process is based on the diffusion of species (N^+, N_2^+ and O^+) through the Si matrix, the Si atoms can be either two-, three-, or four-fold coordinated with different combinations of N and O. Therefore, the creation of SiON layer complicates the Si2p peak decomposition. Firstly, the Si-Si contribution corresponding to the substrate is detected at a BE of 99.6 eV [23,28,29]. Then, to monitor surface evolution during the nitridation reliably, we choose to assemble the other contributions in three components illustrated on figure 2 and described as follows. A contribution named $Si(O_x,N_y)$ shifted by +1.1 eV from the Si-Si contribution gathers poor stoichiometric silicon oxynitride SiO_xN_y with $x+y<0.5$ [23,28]. A second contribution shifted by +2.4 eV from Si-Si contribution, corresponds to silicon oxynitride SiO_xN_y with $y>x$ and

x+y>1 [23,28]. This contribution is named $SiON_{rich}$. Finally, a contribution shifted by +3.2 eV from the Si-Si contribution corresponds to silicon oxynitride SiO_xN_y with a high oxygen concentration (x≥y and x+y>1) [23]. This contribution is named $SiNO_{rich}$. The N1s contribution is detected at 398.1 eV for all the sample sets. It is named N-Si(O,N) and ascribed to silicon oxynitride previously described and observed in [28]. Indeed, the BE of this peak is hardly influenced by the chemical environment of its second neighbors. Hence this peak was chosen as a reference peak for binding energy calibration. Another contribution at 399.5 eV corresponding to N-O bond is also observed in N1s [30–32]. Note that no contribution corresponding to $N\text{-}Si_3$ at 397.7 eV is detected [33]. Due to a residual oxygen contamination during the nitridation process, a very weak O_{1s} peak is recorded and can be described as one peak which is ascribed to O-N and/or O-Si bonds in agreement with their very close BE of 532.5 eV and 532.7 eV, respectively [28].

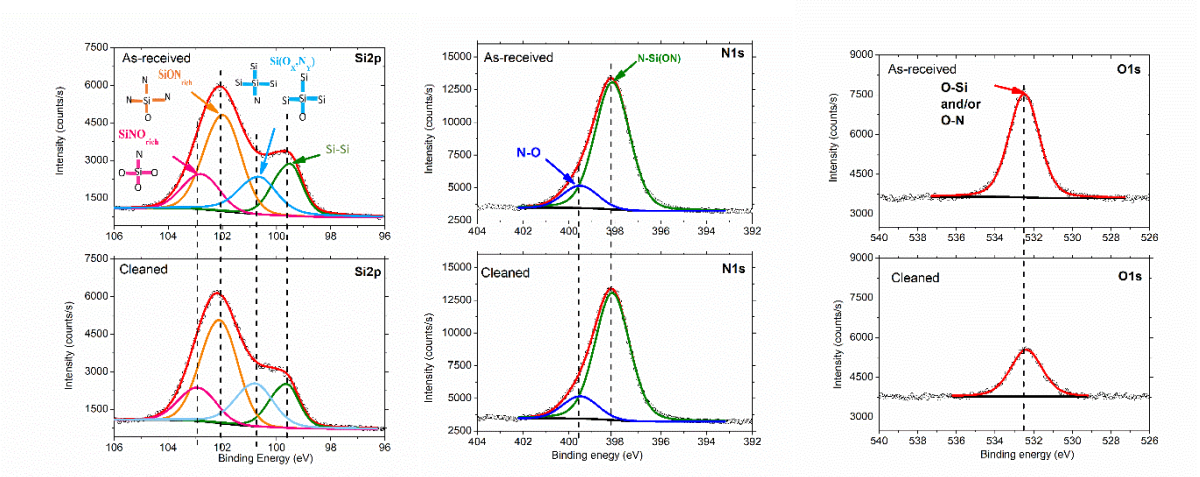

Figure 2: Si2p, N1s and O1s peaks decomposition after 1 h of nitridation at RT of an as-received and cleaned Si(100), acquired at an emission angle of 0°.

Decomposition parameters for Si2p, N1s and O1s peaks have been summarized in Table 1. As no LEED pattern has been observed indicating that the nitride film created is amorphous, the full width at half maximum (FWHM) of Si-Si contribution from the Si crystalline substrate

is lower than the FWHM of contributions corresponding to the amorphous silicon nitride film. This decomposition methodology has been applied to all the samples for all the recorded emission angles.

Table 1: Binding Energy and FWHM optimal parameters of each contribution for Si2p, N1s and O1s spectra.

	BE (eV)	FWHM	Name
Si2p	99.6	1	Si-Si [23,28–30]
	100.7	1.45	$Si(O_x,N_y)$[23,28]
	102	1.45	$SiON_{rich}$ [23,28]
	102.8	1.45	$SiNO_{rich}$ [23]
N1s	398.1	1.6	N-Si(O,N) [28]
	399.5	1.6	N-O [30–32]
O1s	532.6	1.8 - 2	O-Si and/or O-N [28]

3.2 Modeling of ARXPS signal intensities:

Angle-resolved photoemission of the Si2p peak was carried out to determine the depth distribution of the various Si species ($SiON_{rich}$, $SiNO_{rich}$, $Si(O_x,N_y)$) into the silicon nitride layers.

Evolution of area ratios for each component of the Si2p versus the emission angle is plotted on figure 3 for chemically cleaned Si (100) and Si (111) nitrided for 1h at RT. The area ratios of $SiON_{rich}$ and of $SiNO_{rich}$ contributions relative to Si-Si contribution increase with photoelectron emission angle, therefore suggesting that these contributions are located at the top surface of the nitride layer. However, the area ratio of $Si(O_x,N_y)$ contribution relative

to Si-Si contribution remains constant with emission angle. This observation allows us to conclude that these contributions are located near the interface which created a non-stoichiometric interfacial nitride layer.

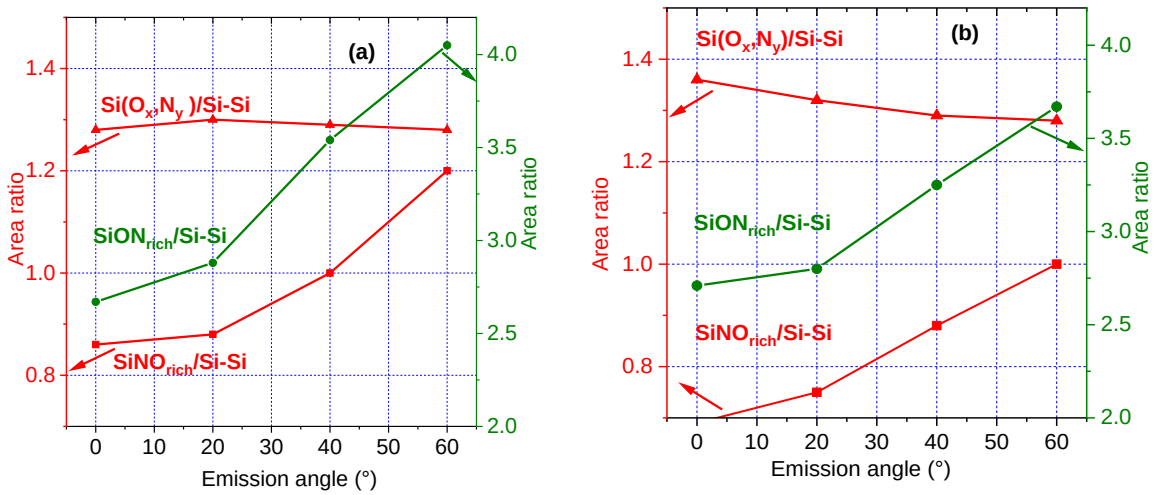

Figure 3: Area ratios of $Si(O_x,N_y)$, $SiON_{rich}$ and $SiNO_{rich}$ intensities relative to Si-Si peak versus photoelectron emission angle for 1 h of nitridation at RT for chemically cleaned (a) Si(100) and (b) Si(111).

Based on Fadley's formula [25], the photoelectron signal intensity due to a thin layer at a depth z is given by the following expression:

$$\mathrm{I_A} = \phi.\,\mathrm{F_c}(\mathrm{E_k}).\,\mathrm{L_A}.\,\sigma_\mathrm{A}.\int_0^\infty \mathrm{N_A}(\mathrm{z}).\exp\left(\frac{-\mathrm{z}}{\lambda_\mathrm{i}^\mathrm{B}(\mathrm{E_C}).\,\cos\theta}\right)\mathrm{dz} \qquad \text{Eq. (A.1)}$$

Where φ is the flux of X-ray photons

$\mathrm{F_c} = T(E_k).A(E_k)$ corresponds to the correction function of the analyzer which depend on the transmission efficiency of the analyzer $T(E_k)$ and the analysis area $A(E_k)$ at the kinetic energy $\mathrm{E_k}$. In our case: $T(E_k) = E_k^{0.59}$ and $A(E_k) = E_k^{-1.21}$ [34].

σ_A is the photoemission cross-section calculated by J.H.Scofield [35].

L_A is the orbital angular symmetry factor: $L_A = 1$ at 54.7° the "magic angle".

$\mathrm{N_A(z)}$ is the atomic density (number of atoms in unit volume) of element A at depth z.

$\lambda_i^B(E_k)$ is the inelastic mean path (IMFP) of the photoelectron having a kinetic energy E_k travelling the material B [36].

Taking into account the previous observations, the growth film can be modeled by two $Si_{xi}N_{yi}O_{zi}$ layers with different thickness and chemical composition as presented in Figure 4, where layer i=1 corresponds to the near surface region of the silicon nitride film and layer i=2 corresponds to the interfacial layer. Then, the theoretical signal intensities of each peak can be calculated for all the measured emission angles (0°, 20°, 40° and 60°). This approach is similar to the studies carried out in [37,38].

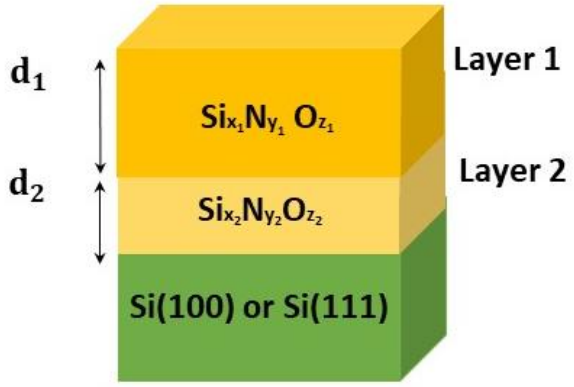

Figure 4: Schematic illustration of a bi-layer model where xi, yi, zi are the stoichiometry coefficients and di is the thickness of the near surface layer (i=1) and the interfacial layer (i=2) describing the silicon nitride thin film deposited on Si substrates.

For the Si2p peak, the total photoelectron signal is the sum of 3 signal intensities:

$$I_{Si2p} = I_{Si2p}^{Si} + I_{Si2p}^{layer1} + I_{Si2p}^{layer2} \qquad \text{Eq. (A.2)}$$

Where I_{Si2p}^{Si} is from the silicon substrate, I_{Si2p}^{layer1} corresponding to the signal intensity of layer 1 and I_{Si2p}^{layer2} corresponds to the signal intensity of layer 2.

The Si2p signal intensity from the silicon substrate is attenuated by the thickness d_1 of layer 1 and d_2 of layer 2 and is given by:

$$I_{Si2p}^{Si} = \phi . F_c(E_k) . \sigma_{Si} . \int_0^{\infty} N_{Si} \exp\left(\frac{-d_1}{\lambda_{Si}^{layer1} . \cos\theta}\right) \exp\left(\frac{-d_2}{\lambda_{Si}^{layer2} . cos\theta}\right) \exp\left(\frac{-z}{\lambda_{Si}^{Si} . cos\theta}\right) dz$$

Eq. (A.3)

On integration of Eq. A.3 and considering that $\lambda_{Si}^{SiNO} = \lambda_{Si}^{layer1} = \lambda_{Si}^{layer2}$ and $N_{Si} = 1$, the Si2p intensity is given by:

$$I_{Si2p}^{Si} = \phi . F_c(E_k) . \sigma_{Si} . N_{Si} . \lambda_{Si}^{Si} . \cos\theta . \exp\left(\frac{-(d_1+d_2)}{\lambda_{Si}^{SiNO} . cos\theta}\right)$$ Eq. (A.4)

The Si2p intensity provided by layer 1 attenuated by the thickness d_2 of layer 2 and Si2p intensity provided by the layer 2 attenuated by the thickness d_1 of layer 1 are given by:

$$I_{Si2p}^{layer1} = \phi . F_c(E_k) . \sigma_{Si} . x_1 . \lambda_{Si}^{SiNO} . cos\theta \left(1 - \exp\left(\frac{-d_1}{\lambda_{Si}^{SiNO} . \cos\theta}\right)\right)$$ Eq. (A.5)

$$I_{Si2p}^{layer2} = \phi . F_c(E_k) . \sigma_{Si} . x_2 . \lambda_{Si}^{SiNO} . \cos\theta . \exp\left(\frac{-d_1}{\lambda_{Si}^{SiNO} . \cos\theta}\right) . \left[1 - \exp\left(\frac{-d_2}{\lambda_{Si}^{SiNO} . \cos\theta}\right)\right]$$

Eq. (A.6)

Where x_1 and x_2 correspond to the silicon concentration of each layer which varies between [0-1].

The theoretical signal intensities of N1s and O1s are calculated with the same approach. And a MATLAB code was developed to find a numerical estimation of the different parameters (x_i,y_i,z_i,d_i) by combining theoretical and experimental results of the XPS intensities. The theoretical intensity ratios $\frac{I_{N1s}}{I_{\mathrm{Si2p}}}$, $\frac{I_{O1s}}{I_{\mathrm{Si2p}}}$ and $\frac{I^{i}_{Si2p}}{I^{Si}_{Si2p}}$ (with i = Si(O_x,N_y), $SiON_{rich}$, $SiNO_{rich}$) are calculated for all the possible combinations of parameters in the range of 0-1 for x_i, y_i and z_i (with a step size of 0.01) and in the range of 0-10 nm for d_i. Then, all these combinations for all emission angles are compared with the experimental ones. Only the combinations having a deviation of less than +/- 10% from the experimental result are considered. Then an average value of each parameter (x_i,y_i,z_i,d_i) is calculated. The error bar of +/- 10% corresponds to uncertainties of parameters used for quantitative XPS analysis. Two constraints consistent with the Si2p decomposition have also been applied in the code to reduce the number of solutions. Firstly, ARXPS interpretations deduced lower Si concentration in layer 1 than in layer 2 ($x_1<x_2$). Secondly, layer 2 is composed of a poor stoichiometric silicon oxynitride film corresponding to $x_2 \leq 0.66$ as mentioned in [23].

A cross sectional HR-TEM image of the SiN_x film deposited on cleaned Si (100) at 500°C for 3h is shown in Figure 5. The silicon nitride layer thickness is measured at about 7.1 nm. This result is in good agreement with the thickness estimated by the bilayer model (7.3 nm) presented below (Table 3).

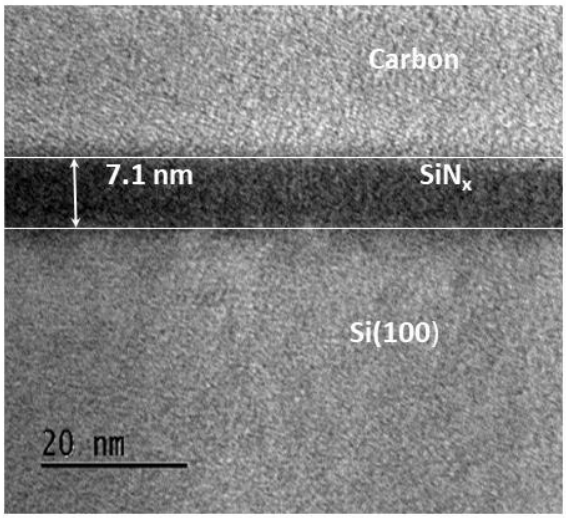

Figure 5: A cross sectional HR-TEM images of SiN_x films deposited on silicon (100) at 500°C for 3h.

4. Results:

Si (100) and Si (111), as-received and cleaned, were nitrided at RT and 500°C for 1h. The chemical composition and estimated thickness of the surface region (layer 1) and the interfacial layer (layer 2) obtained from the XPS signal modeling are summarized in Table 2.

Table 2: Chemical composition and thickness estimations obtained by the bi-layer modeling for as-received and cleaned Si(100) and Si(111) nitrided during 1h at RT and 500°C.

			Layer 1 : Top surface region				Layer 2 : Interfacial layer				Total thickness
			Si%	N%	O%	d_1(nm)	Si%	N%	O%	d_2(nm)	d(nm)
RT	Si(100)	As received	45	50	5	3.1	60	10	30	2.8	5.9
		Cleaned	45	50	5	3.6	60	10	30	2.9	6.5
	Si(111)	As received	45	45	10	3.1	60	25	15	2.8	5.9
		Cleaned	45	50	5	3.1	60	25	15	2.8	5.9
500°C	Si(100)	As received	50	50	0	3.5	55	5	40	1.2	4.7
		Cleaned	50	50	0	3.7	60	25	15	1.3	5
	Si(111)	As received	50	45	5	3.7	60	30	10	1.1	4.8
		Cleaned	50	45	5	3.7	60	35	5	1.3	5

4.1 Influence of the initial surface state and the crystallographic orientation:

In this section, we study the impact of initial state of the Si surface and its crystallographic orientation on the nitridation process. Both sample series are nitrided at room temperature for 1h. The compositions of the two layers remain similar whatever the initial preparation of silicon substrates (as-received or cleaned) for the Si(100) and Si(111) orientations. Furthermore for these two orientations, the top surface layer is composed mainly of Si (45%) and N (45-50%) species, and a small quantity of oxygen (5-10%). The interfacial layer reveals a lower nitrogen concentration of 10% for Si(100) and 25% for Si(111), and an increase of the oxygen concentration reaching 30% for Si(100) and 15% for Si(111). The two layers have comparable thicknesses around 3 nm (Table 2). The difference in chemical composition of the interfacial layer between these two crystallographic orientations reveals that crystallographic compacity affects the diffusion velocities of the different species.

4.2 Influence of the nitridation temperature:

To study the effect of nitridation temperature, the same nitridation processes have been carried out at 500°C for 1h on as-received and cleaned Si(100) and Si(111). For nitridation of Si(100), the top surface layer is composed of 50% of Si and 50% of N whatever the initial state preparation and nitridation temperature. When the nitridation temperature is 500°C, the interfacial layer is richer in nitrogen (25%) than oxygen (15%) for cleaned Si(100). However, a small quantity of nitrogen (5%) and a high oxygen fraction (40%) is observed for as received Si(100) (Table 2). For nitridation of Si (111), at 500°C, the top surface layer is composed of 50% of Si and 45% of N with a small amount of oxygen (5%) which is similar to results obtained for RT nitridation. Whatever the initial surface state, a slight enrichment in nitrogen is detected in the interfacial layer when the temperature is increased to 500°C (Table 2). The thicknesses of layer 1 remains stable around 3.1-3.7 nm for all experimental configurations (i.e. the Si crystallographic orientation, the initial surface preparation and the nitridation temperature). Conversely, the thickness of the interfacial layer obtained at 500°C is around half that for nitridation at RT. This leads to a lower total thickness of the nitrided silicon film at 500°C by at least 1 nm than for RT nitridation (Table 2). The interfacial layer thickness decreasing at 500°C shows that the interface becomes more abrupt. Moreover, decreasing oxygen concentration at the interface layer at 500°C for both crystallographic orientations seem difficult to explain at first sight. We therefore study in the next section the kinetics of this nitridation process at high temperature.

4.3 Evolution of thickness and chemical composition of the silicon nitride film with nitridation time:

To study the nitridation kinetics, the nitridation of cleaned Si (100) at 500°C was studied for the following durations: 10 min, 1h, 3h, and 6h. The chemical composition and thickness of silicon nitride films are summarized in Table 3. The surface layer composition is unchanged for all nitridation times and its composition is close to 50% Si and 50% N species. A significant increase of oxygen concentration in the interfacial layer with nitridation time is observed from 5% to 35% (Table 3). For the 6h nitrided sample, the interfacial composition obtained by the bi-layer modeling is likely to be wrong or misleading as the XPS analysis depth limit is reached (considered to be $3\lambda_{Si}^{SiON}$).

Table 3: Chemical composition and thickness estimations calculated by the bi-layer modeling versus nitridation time for a cleaned Si (100) nitrided at 500°C.

Nitridation time	Layer 1: Top surface region				Layer 2: Interfacial layer				
	Si %	N %	O %	d_1 (nm)	Si %	N %	O %	d_2 (nm)	$d = d_1 + d_2$ (nm)
10 min	50	45	5	0.8	60	35	5	0.7	1.5
1h	50	50	0	3.7	60	25	15	1.3	5
3h	50	50	0	5.5	60	5	35	1.8	7.3
6h	50	50	0	6.3	-	-	-	2	8.3

Evolution of the total thickness of the nitride layer versus the nitridation time is plotted in Figure 6. The quasi-saturation of the nitridation process was not reached even after 6h of nitridation.

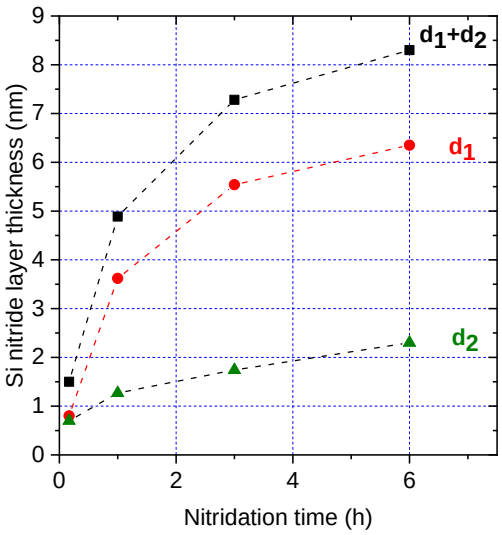

Figure 6: Evolution of estimated thickness of the nitride layer versus nitridation time at 500°C on cleaned Si (100) substrate.

5. Discussions:

From the results section, the nitridation process is mainly based on the diffusion and reaction of N_2^+, N^+ and O^+ species produced by the GDS from the region of higher concentration to the region of lower concentration. These ion species become neutralized when they reach the Si surface, conserving their kinetic energy as observed in [10]**.** We will try to describe the nitridation phenomena taking place in a simultaneous and competitive way. These phenomena which occur during the nitridation process are summarized in figure 7.

In the case of the as-received Si surface, during the first steps of the nitridation process, nitrogen species are incorporated into the silicon oxide. This incorporation is accompanied by oxygen atom substitution. Thus, a part of this oxygen present in the silicon oxide layer migrates to the surface and desorbs as NO and/or O_2 species as observed in [39,40], or may diffuse in the Si matrix. This deoxidation is enhanced when the nitridation temperature

increases as shown in Table 2. Then, for all the samples (as received or deoxidized), the nitrogen species react with the Si surface to form silicon nitride films.

The oxygen ions present in the plasma can react with nitrogen ions in layer 1 leading to formation of NO species in layer 1 and desorb at the surface as observed by Song *et al.*[41]. This phenomenon leads to a low oxygen concentration in layer 1 compared to layer 2 and is enhanced by the nitridation temperature as shown in Table 2. However, oxygen species from contamination of the GDS source and/or from the native SiO_2 surface layer [40] can also migrate to the SiN/Si interface to form a layer 2 richer in oxygen than layer 1. These interpretations are strengthened by the fact that oxygen diffusivity is faster than that of nitrogen in silicon nitride at RT as observed in [42].

When the nitridation temperature increases, the diffusivity and reactivity of N^+, N_2^+ and O^+ species improve [43,44]. However, the oxygen concentration decreases within layer 2 (Table 2), suggesting an enhancement of oxygen desorption as NO species with temperature. This phenomenon explains the lower thickness of layer 2 and therefore the abrupt interface for high temperature nitridation.

The silicon orientation also influences the nitridation process since a higher concentration of nitrogen relative to oxygen in layer 2 in the case of (111) compared to (100) orientation (Table 2) is observed. This is explained by faster diffusivity of nitrogen as observed in [45], where a low diffusion barrier for nitrogen species in Si_3N_4 deposited on Si (111) is determined by Density Functional Theory (DFT) calculations.

Increasing the nitridation time leads to an increase of the nitrided layer thickness, as shown in Figure 6. However, even if the growth rate sharply decreases during nitridation, quasi-saturation of the nitride layer is not reached. Wu *et al.* [46] obtained quasi-saturation in a shorter time and explained it by a very low diffusion length of the nitrogen in a high-density Si_3N_4 film created during the nitridation which prevents nitrogen from reaching the interface. In our case, the amorphous synthesized SiN_x overlayer is less dense than the Si_3N_4, so it takes longer to reach quasi-saturation. These observations further reinforce the fact that the predominant phenomenon during the nitridation process is the diffusion of nitrogen and oxygen species into silicon.

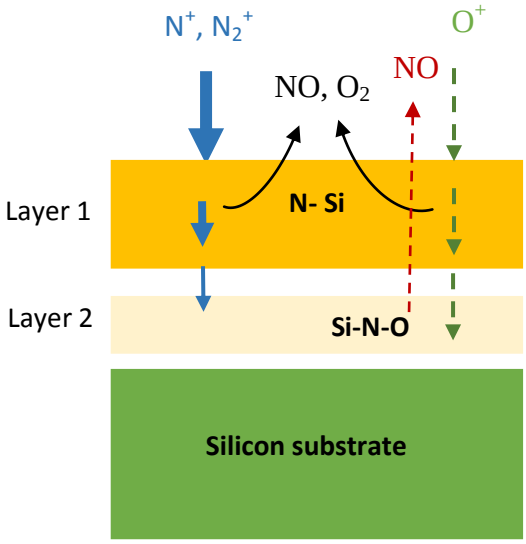

Figure 7: Schematic illustration of the various phenomena occurring during the nitridation process (the red arrow indicates additionally NO desorption from layer 2 at 500°C for clean Si (100)).

6. Conclusion:

The nitridation of both as-received and cleaned Si (100) and Si (111) surfaces under various conditions was investigated by ARXPS, a powerful tool for nondestructive depth profiling in the nanometer range. To improve ARXPS data interpretation, the ARXPS intensities are used

to build a bi-layer surface model to determine the depth chemical composition and the thickness of the silicon nitride film. During the nitridation process, an equilibrium is established between numbers of N and Si atoms in layer 1, whatever the development parameters. Conversely, the interfacial layer composition and thickness are influenced by Si orientation, chemical surface cleaning and nitridation temperature. The presence of oxygen in the nitride film is due to either source contamination or the silicon native oxide. These results allow us to understand the various mechanisms occurring during the nitridation process. The silicon nitride growth is governed by diffusion of nitrogen in the silicon matrix. Due to the presence of oxygen, an NO desorption phenomenon competes with diffusion leading to low oxygen content in layer 1. Therefore, to obtain a more abrupt interface with low oxygen content in layer 2, a high nitridation temperature (500°C) is useful in the case of cleaned Si(100) and (111) surfaces. Moreover, the cleaned Si (111) surfaces exhibit significantly lower oxygen incorporation in the nitrided film regardless of the nitridation temperature when compared to Si (100).

Acknowledgement:

The authors also want to thank E. Gardés and J. Colombet for their contributions on the FIB-HR-TEM analyses.

Funding:

This work was sponsored by a public grant overseen by the French National Research Agency as part of the “Investissements d’Avenir” through the IMobS3 Laboratory of Excellence (ANR-10-LABX-0016) and the IDEX-ISITE initiative CAP 20-25 (ANR-16-IDEX-0001).

References:

[1] M. Raugei, P. Frankl, Life cycle impacts and costs of photovoltaic systems: Current state of the art and future outlooks, Energy. 34 (2009) 392-399. https://doi.org/10.1016/j.energy.2009.01.001

[2] S. Ranjan, S. Balaji, R.A. Panella, B.E. Ydstie, Silicon solar cell production, Comput. Chem. Eng. 35 (2011) 1439-1453. https://doi.org/10.1016/j.compchemeng.2011.04.017

[3] H.K. Raut, V.A. Ganesh, A.S. Nair, S. Ramakrishna, Anti-reflective coatings: A critical, in-depth review, Energy Environ. Sci. 4 (2011) 3779-3804. https://doi.org/10.1039/c1ee01297e

[4] S. Hasegawa, M. Matuura, Y. Kurata, Amorphous SiN:H dielectrics with low density of defects, Appl. Phys. Lett. 49 (1986) 1272-1274. https://doi.org/10.1063/1.97383

[5] T. Tachibana, D. Takai, T. Kojima, T. Kamioka, A. Ogura, Y. Ohshita, Minority Carrier Recombination Properties of Crystalline Defect on Silicon Surface Induced by Plasma Enhanced Chemical Vapor Deposition, ECS J. Solid State Sci. Technol. 5 (2016) Q253-Q256. https://doi.org/10.1149/2.0371609jss

[6] J. Schmidt, A.G. Aberle, Carrier recombination at silicon-silicon nitride interfaces fabricated by plasma-enhanced chemical vapor deposition, J. Appl. Phys. 85 (1999) 3626-3633. https://doi.org/10.1063/1.369725

[7] J. Schmidt, M. Kerr, A. Cuevas, Surface passivation of silicon solar cells using plasma-enhanced chemical-vapour-deposited SiN films and thin thermal SiO_2/plasma SiN stacks, Semicond. Sci. Technol. 16 (2001) 164-170. https://doi.org/10.1088/0268-1242/16/3/308

[8] C. Zhou, J. Zhu, S.E. Foss, H. Haug, Ø. Nordseth, E.S. Marstein, W. Wang, SiO_yN_x/SiN_x

stack Anti-reflection Coating with PID-resistance for crystalline silicon solar cells, Energy Procedia. 77 (2015) 434-439. https://doi.org/10.1016/j.egypro.2015.07.061

[9] A. Markwitz, H. Baumann, W. Grill, A. Knop, E.F. Krimmel, K. Bethge, Investigations of ultrathin silicon nitride layers produced by low-energy ion implantation and EB-RTA, Nucl. Inst. Methods Phys. Res. B. 89 (1994) 362-368. https://doi.org/10.1016/0168-583X(94)95201-9

[10] K.H. Park, B.C. Kim, H. Kang, Silicon nitride formation by low energy N^+ and N_2^+ ion beams, J. Chem. Phys. 97 (1992) 2742-2749. https://doi.org/10.1063/1.463064

[11] K. Ando, A. Ishitani, K. Hamano, Ultrathin silicon nitride films prepared by combining rapid thermal nitridation with low-pressure chemical vapor deposition, Appl. Phys. Lett. 59 (1991) 1081-1083. https://doi.org/10.1063/1.106350

[12] A.G. Schrott and S.C. Fain Jr, Nitridation of Si(111) by nitrogen atoms. II, Surf. Sci. 123 (1982) 204-222. https://doi.org/10.1016/0039-6028(82)90323-5

[13] H. Nakamura, M. Kaneko, S. Matsumoto, S. Fujita, A. Sasaki, Thermal nitridation of silicon in nitrogen plasma, Appl. Phys. Lett. 43 (1983) 691-693. https://doi.org/10.1063/1.94447

[14] H. Zhu, D. Yang, L. Wang, D. Due, Thermal nitridation kinetics of silicon wafers in nitrogen atmosphere during annealing, Thin Solid Films. 474 (2005) 326-329. https://doi.org/10.1016/j.tsf.2004.09.006

[15] S.M. Chérif, J.P. Lacharme, C.A. Sébenne, Surface properties of Si(100)2 × 1 upon NH_3 adsorption and vacuum annealing, Surf. Sci. 262 (1992) 33-41. https://doi.org/10.1016/0039-6028(92)90457-H

[16] J.L. Bischoff, L. Kubler, D. Bolmont, C.A. Sébenne, J.P. Lacharme, J.E. Bonnet, K Hricovini, A photoemission study of ammonia adsorption on Si(100)2 × 1 and Si(111)2

× 1 surfaces, Surf. Sci. 293 (1993) 35-40. https://doi.org/10.1016/0039-6028(93)90240-K

[17] S.P. Murarka, C.C. Chang, and A.C. Adams, Thermal Nitridation of Silicon in Ammonia Gas : Composition and Oxidation Resistance of the Resulting Films, J. Electrochem. Soc. 126 (1979) 996-1003. https://doi.org/10.1149/1.2129223

[18] P. Temple-Boyer, C. Rossi, E. Saint-Etienne, E. Scheid, Residual stress in low pressure chemical vapor deposition SiN_x films deposited from silane and ammonia, J. Vac. Sci. Technol,16 (1998) 2003-2007. https://doi.org/10.1116/1.581302

[19] R. Sahu, S. Palei, J. Choi, Hyung Yong.Y. Ji, K. Kim, Silicon solar cells with nitrogen-rich SiN_x/Si interfacial passivation by low-energy nitrogen-ion implantation, Sol. Energy Mater Sol. Cells. 220 (2021) 110858 1–17. https://doi.org/10.1016/j.solmat.2020.110858

[20] D.A. Shirley, High-resolution x-ray photoemission spectrum of the valence bands of gold, Phys. Rev. B. 5 (1972) 4709-4714. https://doi.org/10.1103/PhysRevB.5.4709

[21] A. Herrera-Gomez, M. Bravo-Sanchez, O. Ceballos-Sanchez, M.O. Vazquez-Lepe, Practical methods for background subtraction in photoemission spectra, Surf. Interface Anal. 46 (2014) 897-905. https://doi.org/10.1002/sia.5453

[22] L. Ley, J. Reichardt, and R.L. Johnson, Static Charge Fluctuations in Amorphous Silicon, Phys. Rev. Lett. 49 (1982) 1664-1667. https://doi.org/10.1103/PhysRevB.41.3284

[23] P. Cova, S. Poulin, O. Grenier, R.A. Masut, A method for the analysis of multiphase bonding structures in amorphous SiO_xN_y films, J. Appl. Phys. 97 (2005) 073518 1-10. https://doi.org/10.1063/1.1881774

[24] M.P. Seah, S.J. Spencer, Ultrathin SiO_2 on Si IV. Intensity measurement in XPS and deduced thickness linearity, Surf. Interface Anal. 35 (2003) 515-524.

https://doi.org/10.1002/sia.1565

[25] C.S. Fadley, Angle-resolved x-ray photoelectron spectroscopy, Prog. Surf. Sci. 16 (1984) 275-388. https://doi.org/10.1016/0079-6816(84)90001-7

[26] H. Mehdi, G. Monier, P.E. Hoggan, L. Bideux, C. Robert-Goumet, V.G. Dubrovskii, Combined angle-resolved X-ray photoelectron spectroscopy, density functional theory and kinetic study of nitridation of gallium arsenide, Appl. Surf. Sci. 427 (2018) 662-669. https://doi.org/10.1016/j.apsusc.2017.08.002

[27] G. Monier, L. Bideux, C. Robert-Goumet, B. Gruzza, M. Petit, J.L. Lábár, M. Menyhárd, Passivation of GaAs(001) surface by the growth of high quality c-GaN ultra-thin film using low power glow discharge nitrogen plasma source, Surf. Sci. 606 (2012) 1093-1099. https://doi.org/10.1016/j.susc.2012.03.006

[28] G. Dinescu, M. Creatore, M.C.M. van de Sanden, Remote nitridation of silicon surface by Ar/N_2-fed expanding thermal plasma, Surf. Coatings Technol. 174-175 (2003) 370-374. https://doi.org/10.1016/S0257-8972(03)00554-1

[29] W. Hansch, A. Nakajima, S. Yokoyama, Characterization of silicon/oxide/nitride layers by x-ray photoelectron spectroscopy, Appl. Phys. Lett. 75 (1999) 1535-1537. https://doi.org/10.1063/1.124747

[30] J.P. Chang, M.L. Green, V.M. Donnelly, R.L. Opila, J. Eng, J. Sapjeta, P.J. Silverman, B. Weir, H.C. Lu, T. Gustafsson, E. Garfunkel, Profiling nitrogen in ultrathin silicon oxynitrides with angle-resolved x-ray photoelectron spectroscopy, J. Appl. Phys. 87 (2000) 4449–4455. https://doi.org/10.1063/1.373090

[31] J. Seiffe, L. Gautero, M. Hofmann, J. Rentsch, R. Preu, S. Weber, R.A. Eichel, Surface passivation of crystalline silicon by plasma-enhanced chemical vapor deposition double layers of silicon-rich silicon oxynitride and silicon nitride, J. Appl. Phys. 109

(2011) 034105 0-12. https://doi.org/10.1063/1.3544421

[32] G.M. Rignanese, A. Pasquarello, J.C. Charlier, X. Gonze, R. Car, Nitrogen incorporation at Si(001)- SiO_2 interfaces: Relation between N 1s core-level shifts and microscopic structure, Phys. Rev. Lett. 79 (1997) 5174-5177. https://doi.org/10.1103/PhysRevLett.79.5174

[33] M. Matsuoka, S. Isotani, W. Sucasaire, L.S. Zambom, K. Ogata, Chemical bonding and composition of silicon nitride films prepared by inductively coupled plasma chemical vapor deposition, Surf. Coatings Technol. 204 (2010) 2923–2927. https://doi.org/10.1016/j.surfcoat.2010.02.071.

[34] M. Aymen, G. Monier, C. Robert-goumet, L. Bideux, B. Gruzza, Journal of Electron Spectroscopy and New method for the determination of the correction function of a hemisperical electron analyser based on elastic electron images, J. Electron Spectros. Relat. Phenomena. 197 (2014) 80–87. https://doi.org/10.1016/j.elspec.2014.09.010.

[35] J.H. Scofield, hartree-slater subshell photoionization cross-sections at 1254 and 1487 eV, J. Electron Spectros. Relat. Phenomena. 8 (1976) 129–137. https://doi.org/10.1016/0368-2048(76)80015-1.

[36] S. Tanuma, C.J. Powell, D.R. Penn, Calculations of Electron Inelastic Mean Free Paths, Surf. Interface Anal. 21 (1993) 165–176. https://doi.org/10.1002/sia.740210302.

[37] M.P. Seah, I.S. Gilmore, S.J. Spencer, Quantitative XPS: I. Analysis of X-ray photoelectron intensities from elemental data in a digital photoelectron database, J. Electron Spectros. Relat. Phenomena. 120 (2001) 93-111 https://doi.org/10.1016/S0368-2048(01)00311-5.

[38] A. Jablonski, Evaluation of procedures for overlayer thickness determination from XPS intensities, Surf. Sci. 688 (2019) 14-24. https://doi.org/10.1016/j.susc.2019.05.004

[39] T. Mizokuro, K. Yoneda, Y. Todokoro, H. Kobayashi, Mechanism of low temperature nitridation of silicon oxide layers by nitrogen plasma generated by low energy electron impact, J. Appl. Phys. 85 (1999) 2921-2928. https://doi.org/10.1063/1.369633

[40] I.J.R. Baumvol, F.C. Stedile, J.J. Trimaille, S. Rigo, Thermal Nitridation of SiO_2 Films in Ammonia: Isotopic Tracing of Nitrogen and Oxygen in Futher Stages and in Reoxidation, J. Electrochem. Soc. 143 (1996) 2946-2952. https://doi.org/10.1149/1.1837131

[41] H.J. Song, H.J. Shin, Y. Chung, J.C. Lee, M.K. Lee, X-ray absorption and photoelectron spectroscopic study of plasma-nitrided SiO2 film, J. Appl. Phys. 97 (2005) 113711 1-7. https://doi.org/10.1063/1.1927283

[42] P.L.F. Hemment, Silicon on insulator formed by O^+ or N^+ ion implantation, MRS Online Proceedings Library (OPL) 53 (1985) 207-221. https://doi.org/10.1557/PROC-53-207

[43] M. Pagani, Secondary ion mass spectroscopy determination of oxygen diffusion coefficient in heavily Sb doped Si, J. Appl. Phys. 68 (1990) 3726-3728. https://doi.org/10.1063/1.346311

[44] V. Gusakov, Unified model of diffusion of interstitial oxygen in silicon and germanium crystals, J. Phys. Condens. Matter. 17 (2005) S2285-S2291. https://doi.org/10.1088/0953-8984/17/22/017

[45] T.L. Petrenko, V.P. Bryksa, I. V. Dyka, V.P. Kladko, A.E. Belyaev, A. V. Kuchuk, Microscopic mechanisms of Si(111) surface nitridation and energetics of Si_3N_4 /Si(111) interface, Appl. Surf. Sci. 483 (2019) 302-312. https://doi.org/10.1016/j.apsusc.2019.03.239

[46] C.Y. Wu, C.W. King, M.K. Lee, C.T. Chen, Growth Kinetics of Silicon Thermal

Nitridation, J. Electrochem. Soc. 129 (1982) 1559-1563. https://doi.org/10.1149/1.2124207